Collimation Effect of Water Collimator to *D–D* and *D–T* Neutrons

by

KAZUO SHIN, Masamichi AKIMURA and Tomonori HYODO

(Received December 27, 1985)

Abstract

A study of a water collimator is performed for 5-cm and 10-cm diam. cylindrical collimators located in a 100-cm water shield. A point neutron source of *D–D* or *D–T* reactions is located at the entrance to the collimator. Results of the Monte Carlo simulation are analyzed as reference data.

Two parameters are proposed to measure the collimation effects, i.e. scattered neutron flux on the axis of the collimator and the width of the plateau observed in the scattered flux profile. The flux on the axis is analyzed by a single-albedo-scattering model, while the width of the plateau is represented by a single-scattering model in the shied.

The flux on the axis is nearly proportional to the collimator radius. The axial profile of the on-axis flux is closely approximated with an imaginary source assumed at the center of the collimator. The imaginary source reproduces the width of the plateau in the radial profile of the scattered flux.

I. Introduction

The collimation of fast neutrons is a key technique for neutron experiment facilities, where source neutrons are often supplied through a collimator. Hence, the accuracy of the experiments depends on the collimator performance. The collimator problem also appears in the design of irradiation facilities for cancer therapy, or diagnostic holes in burning plasma experimental facilities. The spread of streamed neutrons behind ducts is of interest to shielding designers of nuclear facilities.

Studies on collimator effects for neutrons are seen as a part of shielding experimental facility design[1,2] or neutron source characterization study[3,4], and design of diagnostic holes of burning plasma facilities.[5,6] The methods used in these analyses are classified into three categories, i.e. the experiment[3,4], the Monte Carlo calculation[1,5,6] and the albedo Monte Carlo calculation.[2] The experiment required a geometrical setup of massive collimator systems, so it was

* Department of Nuclear Engineering.

not possible by the experiment to get systematic results for a variety of collimator materials and size. The calculations did not have such constraints. The Monte Carlo approach, however, required a long computing time to get results even for a limited number of cases. Hence, the experiment and the Monte Carlo method were used mainly for a characterzation study of already settled collimators. The albedo Monte Carlo method is a fast calculation method, and is applicable for a systematic study of collimator effects. The disadvantage, however, of this method is in the limitation whereby this method is valuable only at points on the collimator axis. The spatial spread of streamed neutrons after exiting from the collimator cannot be analyzed by this method.

The objectives of this work are to find a simple calculation method which quickly reproduces the collimator effect, i.e. the energy spectrum in the collimated beam, and the spread of the neutron beam as well as to systematically examine the dependence of the effect on geometrical parameters. As an example of practical collimator systems, a water collimator is considered. Water is the most popular shield material for neutrons. A point neutron source of *D–D* or *D–T* reactions is assumed at the center of the entrance mouth to the collimator. Monte Carlo calculations by the pointwise Monte Carlo code CYGNUS[7] are performed repeatedly, and neutron energy and spatial distributions are obtained. These results are used as reference data for a further analysis through which the simple analysis method is derived, and the systematics of the collimation effect is examined.

II. Calculational Method

The collimator which is assumed in this work is a straight cylindrical penetration located in a water shield. A point isotropic neutron source of *D–D* (3 MeV) or *D–T* (15 MeV) reactions is located at the center of the entrance mouth to the cylinder. Fig. 1 shows a geometrical model of the collimator system. The thickness of the water shield is 100 cm, and the diameter of the collimater is 5 cm or 10 cm. The spatial distribution and energy spectrum of neutron fluxes behind the collimator are required. The spread of the neutron

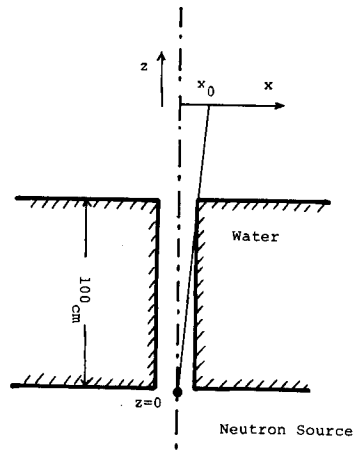

Fig.1 Geometrical configuration of the water duct.

beam and the ratio of direct neutrons from the source to scattered neutrons in the beam are basic parameters which measure the collimator performance.

The Monte Carlo method is employed to simulate the neutron transport through the collimator system. For this purpose, the CYGNUS code, which has been suitable for simple geometry calculations, is modified so that cylindrical duct geometry is included in its geometrical options.

The calculation is done with pointwise cross section data obtained from the ENDF/B-I file.[8] Only the elastic scattering and inelastic scattering with discrete excitation energies are included in the simulation. Other reactions are assumed to be absorption events.

For the improvement of calculational statistics, a source neutron emission is biased with a forward peaked probability and a backward peaked weight. The point detector estimation is employed, i.e. the contribution to neutron fluxes at all detector locations is estimated at every collision point. Absorption events are excluded from the random walk process, and the effect due to the absorption is dealt by the reduction in the neutron weight. A neutron with the weight W transmitted the distance t in the medium, the absorption cross section of which is described as Σ_a. Then, the weight at the end of the path is reduced to $W \exp(-\Sigma_a t)$.

The above Monte Carlo process is summarized by the following equation which describes the neutron energy flux of a detector point in l-th energy group;

$$\Phi_l = \frac{1}{J} F_l \sum_{j=1}^{J} \sum_{k=0}^{L_j} \frac{W_j D_{kj}}{t_{kj}^2} \exp\left(-\Sigma_{t,kj} t'_{kj}\right) \prod_{m=0}^{k-1} \exp\left(-\Sigma_{a,mj} s_{mj}\right), \qquad (1)$$

where W_j = weight of source neutron of j-th history,

D_{kj} = probability of scattering to detector direction at k-th collsion point P_{kj} of the j-th history neutron,

t_{kj} = distance between the detector and point P_{kj},

t'_{kj} = path length of neutron in the medium along the direction from point P_{kj} to the detector,

$\Sigma_{a,kj}$ = absorption cross section,

$\Sigma_{t,kj}$ = total cross section,

s_{mj} = path lenght of the j-th neutron between $(m-1)$-th and m-th collision points,

$$F_l=\begin{cases}1. & E_{l-1}\leq E_n\leq E_l \ (E_n=\text{neutron energy})\\ 0. & \text{otherwise.}\end{cases}$$

Ⅲ. Results of Monte Carlo Simulation

Fig. 2 shows the spatial destribution of neutron fluxes obtained by the Monte Carlo calculations for the case of the 10-cm diam. collimator with the *D-T* neutron source. The parameter "*z*" in the figure means the distance of the detector from the front surface (source side) of the water shield. The horizontal

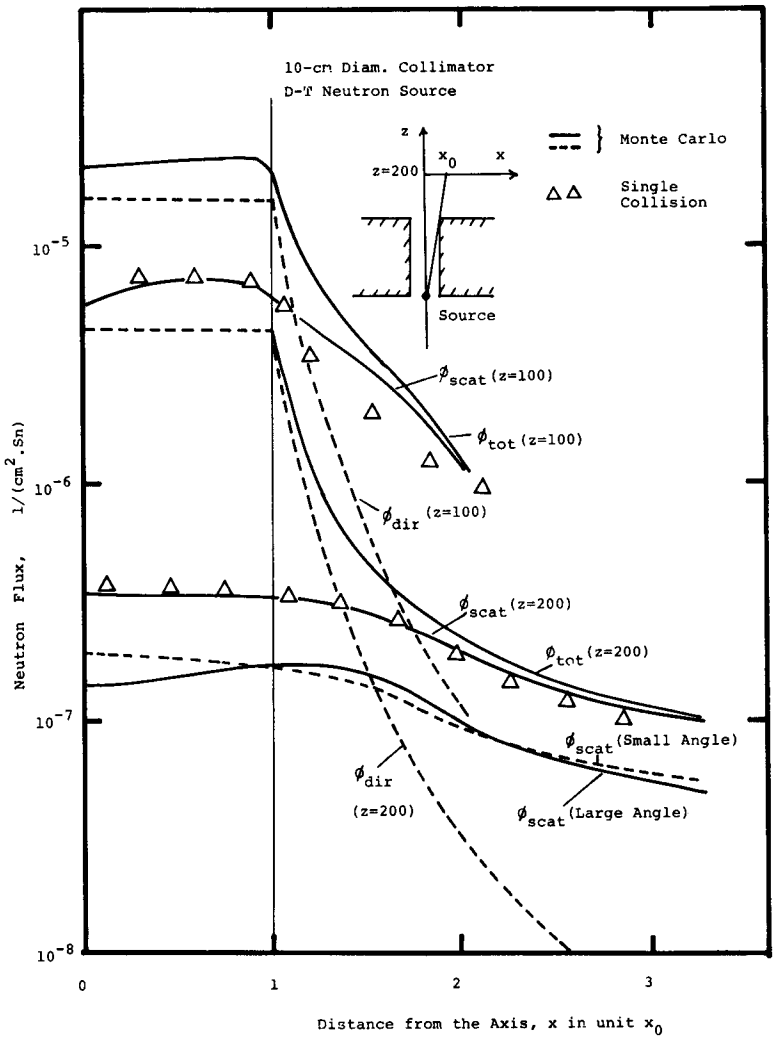

Fig.2 Radial profiles of the total, direct and scattered fluxes for the 10-cm diam collimator with the D-T source.

axis is the location of the detector away from the collimater axis, and is measured in the unit of x_o (See Fig. 1) which is given as

$$x_o = \frac{Z}{100} \times \delta, \tag{2}$$

where δ is the radius of the collimator.

As was expected, the total fluxes are almost uniform within the corn of $x \leq x_o$, (We call this "direct corn."), in which the neutron path from the source to the detector does not pass through water. The fluxes then decrease quickly with

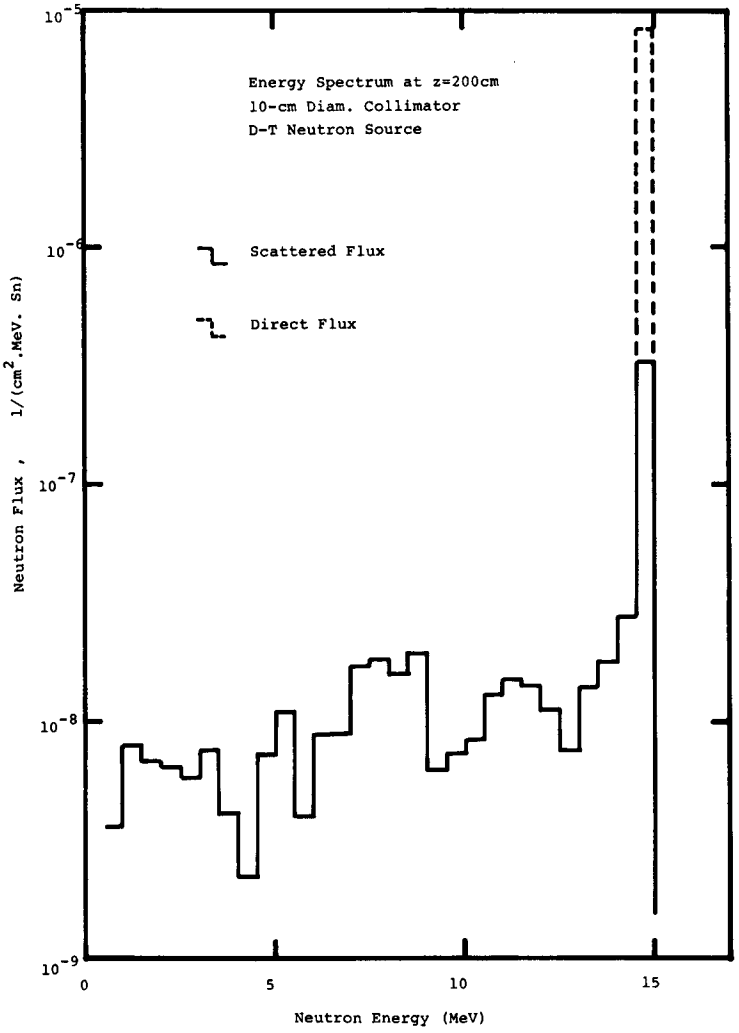

Fig.3 Energe spectrum of collimated neutrons at z=200cm on the collimator axis for the 10-cm diam. collimator with the D-T neutron source.

x as the neutron starts to pass through the water shield. The total flux is broken down into direct and scattered components. It is clear from the figure that the direct component dominates the flux behavior within and near the direct corn, while the scattered component does the same far away from the collimator axis.

Another important observation is that the scattered component also has a plateau like the direct component at the center part of the distribution. It then degrades gradually with the distance x. It is noteworthy that the performance of

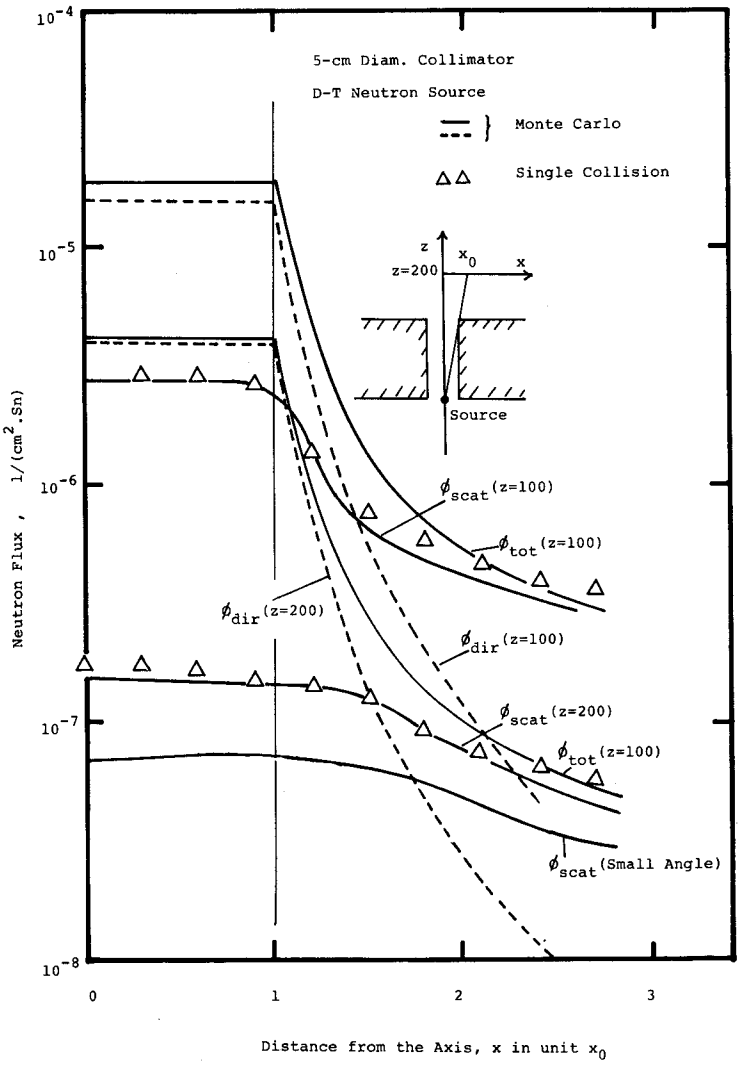

Fig.4 Radial profiles of the total, direct and scattered fluxes for the 5-cm diam. collimator with the D-T source.

the collimator is measured by two factors. One is the ratio of the value for the scattered component to that of the direct component within the direct corn. The less the ratio, the better the collimator. The other is the spread of the neutron flux distribution. Obviously, a sharper distribution is desirable. We will measure this spread by the width of the plateau in the distribution of the scattered component.

Fig. 3 shows the energy spectrum of nerutrons on the collimator axis at $z = 200$ cm for the 10-cm diam. collimator case with the *D-T* source. After excluding the direct component, the specturm still exibits a prominent peak at the energies $14.5 \leq E_n \leq 15$ MeV. The peak is due to the so called "small angle

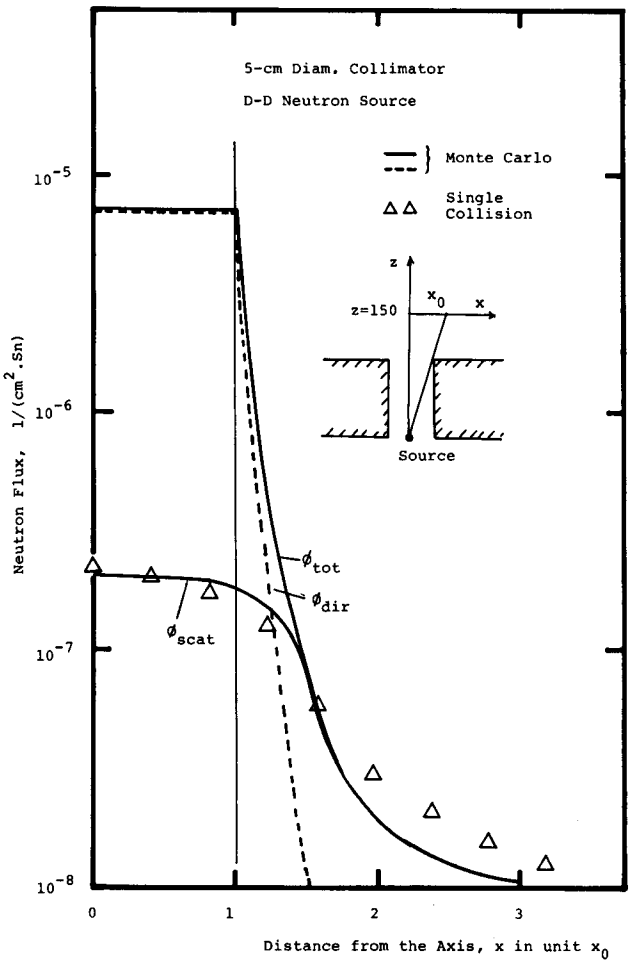

Fig.5 Radial profiles of the total, direct and scattered fluxes obtained at z=150cm for the 5-cm diam. collimator with the D-D source.

scattering" mostly with oxygen nuclei. This peak is separated from the rest of the scattered flux, and is plotted in Fig. 2 together with the other flux. Both the small angle scattering component and the rest closely follow the behavior of the total scattered component. This means the energy spectrum of the scattered cosponent is almost same over the wide region in and around the direct corn.

Figs. 4 and 5 show similar flux distributions for the cases of the 5-cm diam. collimator with the *D-T* and *D-D* neutron sources, respectively. The same things as for Fig. 2 are also pointed out in the figures.

IV. Analysis

It was indicated in the above chapter that the collimation effect was measured by two parameters, i.e. the ratio of the value of the scattered flux to the direct flux, and the width of the plateau in the distribution of the scattered flux. The direct flux is calculated by the equation,

$$\Phi_{dir}=S_o \exp(-\Sigma_t t) / (4\pi l^2), \tag{3}$$

where S_o =source strength,

Σ_t =total cross section of water for source neutrons,

t =path length of source neutrons in the water along the direction from the source to the detector,

l =distance between the source and the detector.

(i) Scattered Flux on Axis

For the estimation of the scattered flux on the collimator axis, the albedo model is applicable where the neutron multiscattering in the water shield is replaced by a single reflection at the collimator wall with a certain reflecting efficiency. Here, we assume that neutrons make scattering only once at the collimator wall.

The scattered flux is evaluated by the following equation:

$$\Phi_{scat}(z) = \int_0^{100} F(z, t) \tag{4}$$

$$F(z, t) = \frac{S_o \delta}{2(t^2+\delta^2)} \cos\theta_1 \alpha f(\theta_2) \frac{1}{(z-t)^2+\delta^2}, \tag{5}$$

where S_o =source intensity,

δ =collimator radius,

α =albedo of water,

and $f(\theta_2)$ =angular dependence of albedos on reflecting polar angle θ_2.

$(2\pi\int_0^{\pi/2} f(\theta_2)\ \sin\theta_2 d\theta_2 = 1.)$

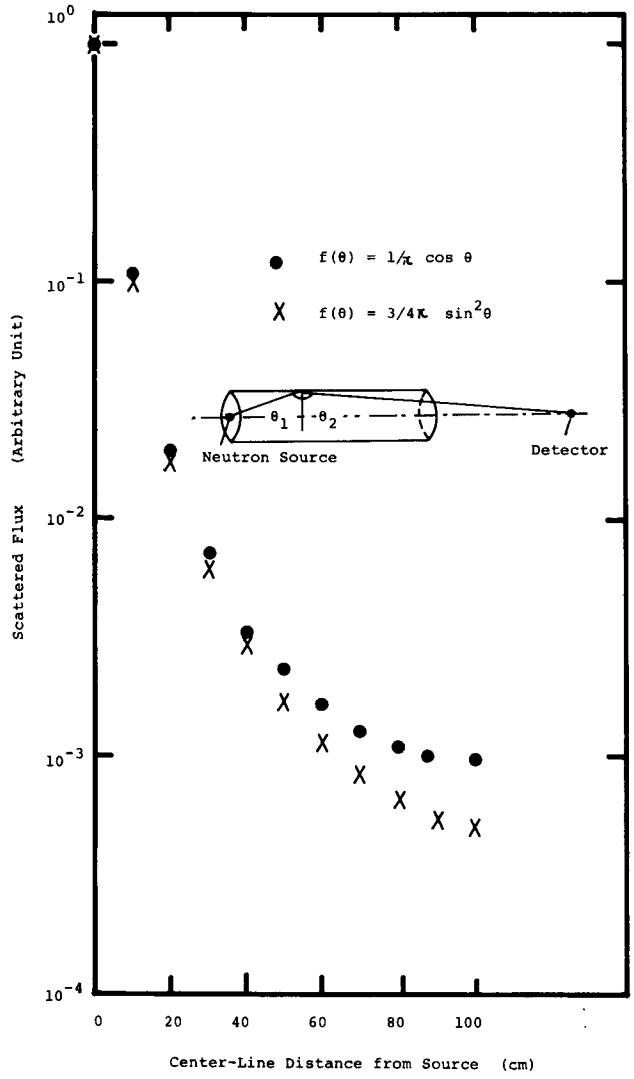

Fig.6 Contoribution to the scattered flux from scattering on the collimator wall at each depth.

The function $f(\theta)$ has not been studied well for water and is unknown. The F function in *Eq.* (5) is tested with two $f(\theta)$ functions; $1/\pi \cos\theta$, and $3/4\pi \sin^2\theta$. The results are shown in Fig. 6 for $z=200$ cm. Not much difference is noticeable in the F function between the two f's. The flux is decided by the scattering only around the neutron source ($z\sim 0$). The $1/\pi \cos\theta$ will be used below for the function f, and then *Eqs.* (4) and (5) are rewritten as *Eq.* (6),

$$\phi_{scat}(Z) = \frac{S_0 \alpha \delta^3}{2\pi} \int_0^{100} \frac{dt}{(t^2+\delta^2)^{3/2}\{(z-t)^2+\delta^2\}^{3/2}}, \qquad (6)$$

Fig. 7 shows the axial distributions of the scattered flux component and the direct component obtained for the *D-T* neutron source by *Eqs.* (6) and (3), respectively. The analytical rusults are normalized to the Monte Corlo value at

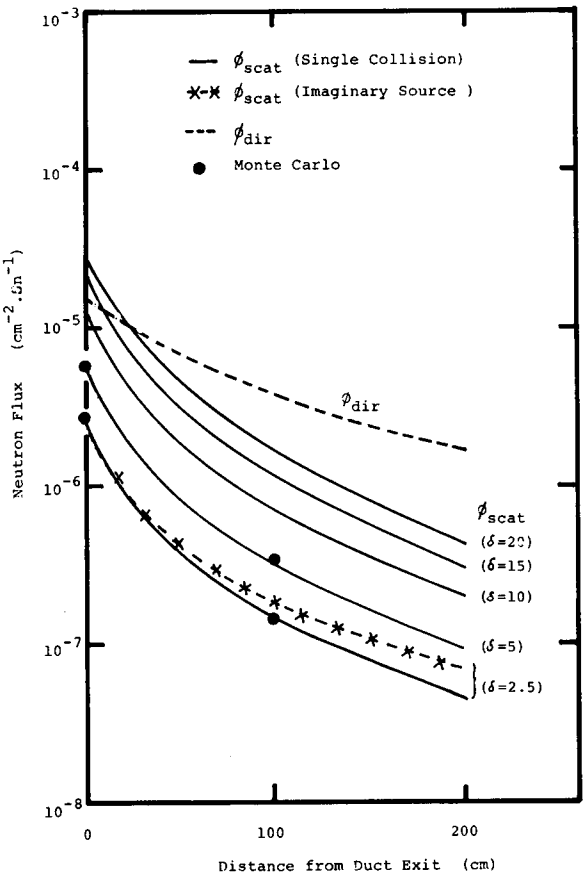

Fig.7 The axial profiles of the scattered and direct fluxes for various collimator radii.

a 100-cm distance from the duct exit of the 10-cm diam. collimator case by considering the albedo as a fitting parameter, e.g. $\alpha = 1.57$. Then, the Monte Carlo results are very well reproduced by the analytical method even in the cases of a different distance (0 cm from the duct exit) and a different collimator diameter (5 cm diameter). It is observed from the figure that the value of the scattered flux component increases with the radius of the collimator, and decreases with the distance of the point from the duct exit. The direct component also decreases as the point moves further from the duct exit, but its decreasing rate is smaller than that of the scattered component. A better collimation performance is obtained, as the spectrum is concerned, with smaller radius collimators and at further points from the duct exit. It is noteworthy that the scattered component dominates near the exit of larger size collimators.

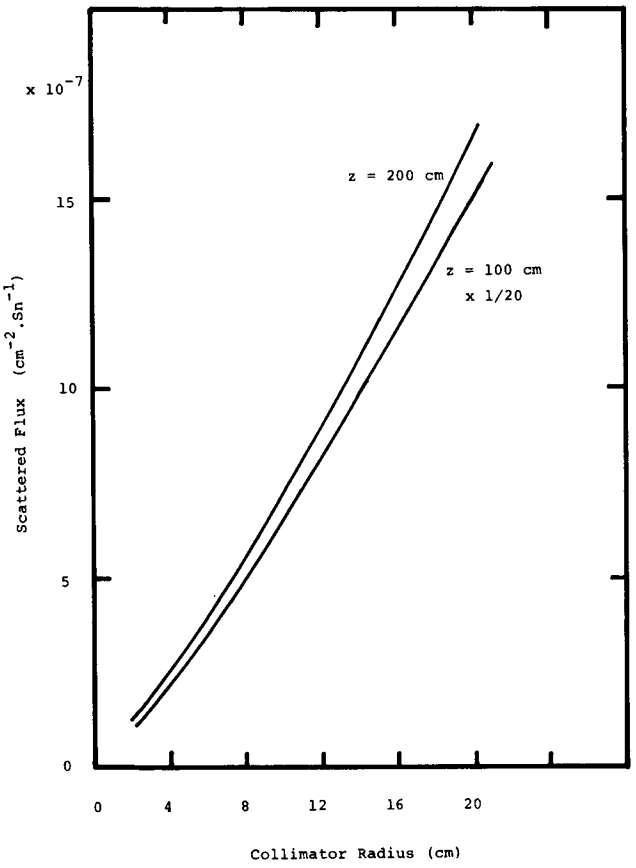

Fig.8 Plot of the scattered flux on the collimator axis vs. the collimator radius δ .

In Fig. 8, the scattered flux is plotted as a function of the collimator size. We can say the scattered flux is nearly proportional to the collimator radius. If the radius is decreased to zero, the scattered flux will approach to a certain very small but not zero value, which corresponds to leakage neutrons through a plane 100-cm water shield.

The same things are pointed out for the *D–D* neutrons. (Not shown in the figures.)

(ii) Beam Spread

For the analysis of the beam spread of the scattered neutrons after exiting from the collimator the single scattering approximation in the wall is used instead of that on the wall of *Eq.* (5). As was pointed out in Fig. 6, most contributions to the scattered flux at points behind the collimator came out from the scattering near the neutron source ($z\sim 0$). Here, the scattering of the source neutrons in the water is considered only on the $z=0$ plane.

$$\phi_{scat}(z) = \int_{S_0} \frac{k\exp\{-\Sigma_r(l_r-\delta)\}}{4\pi l_1^2} \times \frac{\exp(-\Sigma_r t_2)}{l_2^2} ds, \qquad (7)$$

where Σ_r = removal cross section of water for source neutrons,

l_1 = distance of the scattering point from the source,

l_2 = distance of the scattering point from the detector,

t_2 = path length in the water along the direction from the scattering point to the detector,

k = normalization constant,

S_0 = plane $z=0$.

Isotropic scattering is assumed in the above equation, and no energy change in the scattering is considered. The results of the intergration of *Eq.* (7) are shown in Figs. 2, 4 and 5 in comparison with the Monte Carlo rusults. The parameter Σ_r is selected as 0.068 for the *D–T* source, and 0.086 for the *D–D* source to give the best fitting of the curve to the Monte Carlo values. There, k is decided case by case so that the scattered flux values within the direct corn of both calculations agree with each other. The profiles of the scattered neutrons are well reproduced with the simple integral by *Eq.* (7) in all cases. The plateau and the edge of the plateau are very well described by the integral (7).

The profiles of the scattered fluxes in the above figures are differentiated

with the destance x, and the location of a peak in the obtained curves is assigned as the width of the plateau in the profiles. The obtained width R_{eg} is plotted in Fig. 9 as a function of the collimator radius δ for the detector position $z = 200$ cm. There is no clear difference between the R_{eg} values for the *D-D* and *D-T* sources. The width R_{eg} is proportional to the radeus δ. Fig. 10 is the plot of the width R_{eg} vs. the distance from the collimator outlet. Again there are linear relations between these two values. Note that R_{eg} will be zero around the center of the collimator if the curves are extrapolated to the source. Therefore, it will be a good approximation for the estimation of R_{eg} to consider an imaginary point isotropic source at the center of the collimator. Variation of the flux along the collimater axis due to this imaginary source is plotted in Fig. 7, as a function of the distance beyond the collimator exit. The dependence of the scattered flux value on the distance is well reproduced by this approximation, unless the points are very far away the collimator exit.

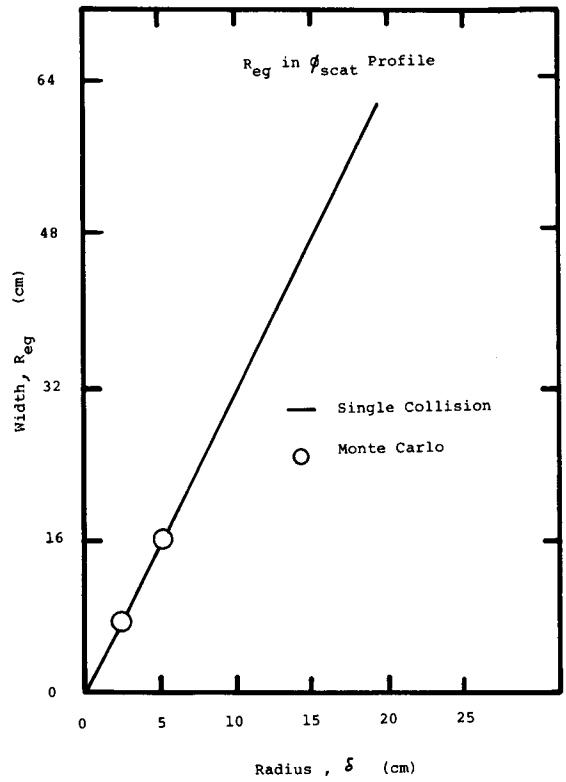

Fig.9 Plateau width R_{eg} in the scattered flux profile as a function of the collimator radius δ .

Summary

The collimation effect of the water collimators to *D-T* and *D-D* neutrons were analyzed, based on the Monte Carlo simulation data. The performance of the collimation effect could be measured by the scattered flux value on the axis of the collimator and the width of the plateau in the scattered neutron profile.

The scattered flux on the axis was estimated by a single collision approximation on the collimator wall. The flux was nearly proportional to the collimator radius.

The width of the plateau was estimated by the single scattering model in the water on the plane $z = 0$ cm. The width R_{eg} was proportional to the collimator radius, and hence, had the linear relation with the distance from the collimator exit.

The imaginary source at the center of the collimator gave a good estimation for the width R_{eg} and the scattered flux profile along the axis.

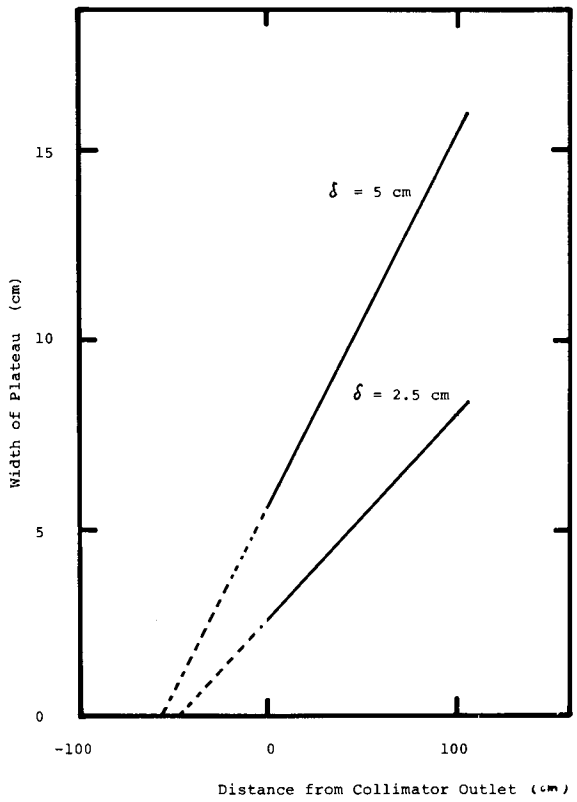

Fig.10 Plot of the plateau width R_{eg} vs. the distance from the collimator outlet for different collimator radii.

Refernces

1) E. A. Straker, "Fast Neutron Collimator Studies," Nucl. Appl. 6, 168 (1969).
2) G. P. deBeer, Nucl. Eng. & Design, 33, 435 (1975).
3) K. Shin, et al., J. of Nucl. Sci. & Technol., 17, 37 (1980).
4) T. Nakamura et al., "Rediation Streaming Studies at the Fusion Neutronics Source (FNS) Facility," Proceedings of the Sixth International Conference on Radiation Shielding, pp. 888, Tokyo Japan (1983).
5) K. Ueki, "Study of Neutron Streaming through Large Shieiding Systems by the Monte Carlo Method," Doctor Thesis, Kyoto University (1984). (in Japanese)
6) J. Kolibal and L. P. Ku, "14 MeV Neutron Streaming through Cylindrical Ducts on the TFTR," Transactions of American Nuclear Society, pp. 776, San Francisco USA (1981).
7) H. Hirayama and Takashi Nakamura, Mem. of Faculty of Engng., Kyoto Univ., Vol. XXXIV, Part 2, 187 (1972).
8) H. C. Honeck: ENDF/B, NBL 50066 (T-467) (1966).